BIOCHEMISTRY
including biophysical chemistry & molecular biology

Article

pubs.acs.org/biochemistry

Ligand-Controlled Assembly of Hexamers, Dihexamers, and Linear Multihexamer Structures by the Engineered Acylated Insulin Degludec

Dorte B. Steensgaard,* Gerd Schluckebier, Holger M. Strauss, Mathias Norrman, Jens K. Thomsen, Anders V. Friderichsen, Svend Havelund, and Ib Jonassen

Diabetes Protein Engineering, Novo Nordisk A/S, Novo Nordisk Park, 2760 Maaloev, Denmark

Supporting Information

ABSTRACT: Insulin degludec, an engineered acylated insulin, was recently reported to form a soluble depot after subcutaneous injection with a subsequent slow release of insulin and an ultralong glucose-lowering effect in excess of 40 h in humans. We describe the structure, ligand binding properties, and self-assemblies of insulin degludec using orthogonal structural methods. The protein fold adopted by insulin degludec is very similar to that of human insulin. Hexamers in the R_6 state similar to those of human insulin are observed for insulin degludec in the presence of zinc and resorcinol. However, under conditions comparable to the pharmaceutical formulation comprising zinc and phenol, insulin degludec forms finite dihexamers that are composed of hexamers in the T_3R_3 state that interact to form an $R_3T_3{-}T_3R_3$ structure. When the phenolic ligand is depleted and the solvent condition thereby mimics that of the injection site, the quaternary structure changes from dihexamers to a supramolecular structure composed of linear arrays of hundreds of hexamers in the T_6 state and an average molar mass, M_0, of 59.7×10^3 kg/mol. This novel concept of self-assemblies of insulin controlled by zinc and phenol provides the basis for the slow action profile of insulin degludec. To the best of our knowledge, this report for the first time describes a tight linkage between quaternary insulin structures of hexamers, dihexamers, and multihexamers and their allosteric state and its origin in the inherent propensity of the insulin hexamer for allosteric half-site reactivity.

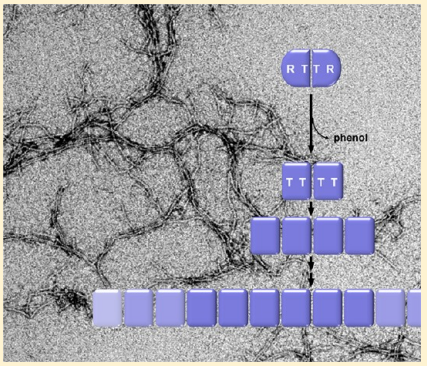

Insulin possesses inherent properties for zinc-mediated hexamer formation, allosteric ligand binding, and conformational changes. For the pharmaceutical use of insulin, the tendency of hexamers to dissociate into monomers influences the rate at which insulin disappears from a subcutaneous injection site and is absorbed into the bloodstream.[1] To match the release of insulin from the injection site to physiological needs, human insulin can be engineered in various ways to tune the release from the injection site and hence the absorption rate. Fast-acting insulin analogues can be achieved by mutations that favor dissociation of the insulin hexamer.[2−4] A protracted pharmacological action profile can be obtained by covalent attachment of albumin binding moieties that aim to prolong circulation in the bloodstream.[5] Besides the primary objective of prolonged circulation caused by albumin binding, there are several examples of the attachment of albumin binders in the form of either cholic acid[6] or fatty acids[7−10] that can alter the self-association properties of pharmaceutically relevant peptides.

Recently, the clinical data for insulin degludec (IDeg), which is a novel acylated insulin that provides an ultralong glucose-lowering effect of beyond 40 h in humans, were reported.[11,12] This acylated insulin is an engineered des(B30) human insulin modified with a hexadecanoic diacid via a γ-L-glutamyl linker to Lys B29 (Figure 1), and it was developed for the purpose of aiming at the formation of a large soluble zinc complex after injection to the sub cutis and the resulting slow release from the injection depot.[13] This report describes the structural properties and ligand binding of the zinc assemblies of insulin degludec that result in an ultralong glucose-lowering effect.

The structure and ligand binding properties of human insulin have been described well (see, e.g., refs 1, 3, and 14). Studies have been motivated by the pharmaceutical relevance of insulin, as well as use of insulin as a model system for allosteric proteins. Human insulin consists of two polypeptide chains. The A-chain (21 amino acids) consists of two short α-helices formed by residues A1−A8 and A13−A19. The B-chain of 30 amino acids is formed around a central helix (B9−B19) flanked by stretches of extended structure at both termini. Two disulfide bridges, A7−B7 and A20−B19, link the two chains covalently. Additionally, there is an intrachain disulfide from A6 to A11. Insulin assembles into dimers, and in the presence of zinc, these dimers readily form globular hexamers that consist of three dimers of insulin arranged around two zinc ions on the 3-fold symmetry axis. Each zinc ion coordinates to three B10 histidine imidazole moieties. Zinc is furthermore coordinated by extrinsic ligands to complete either a tetrahedral or an

Received: June 27, 2012
Revised: December 18, 2012
Published: December 20, 2012

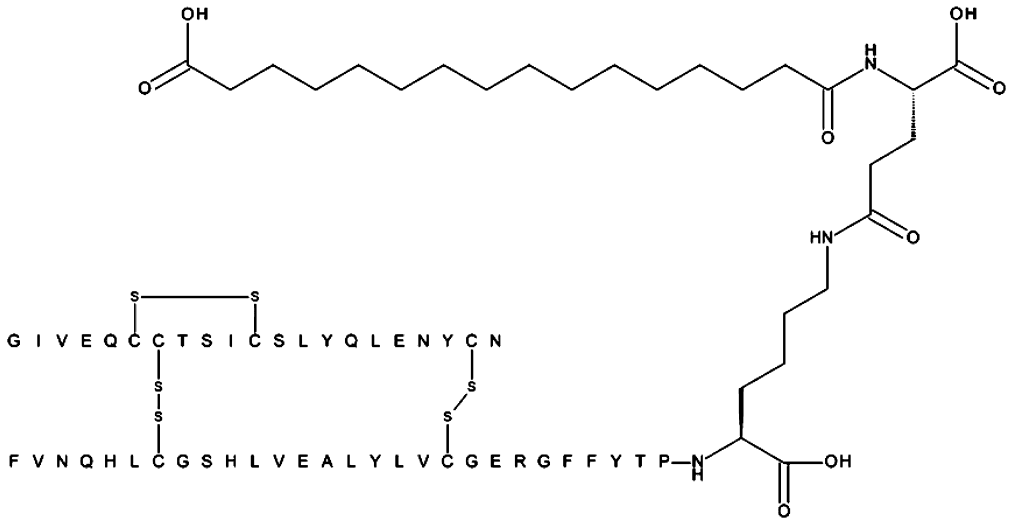

Figure 1. Schematic representation of IDeg. IDeg is des(B30) human insulin acylated at the ε-amino group of Lys B29 with hexadecanoic acid via a γ-L-glutamic acid spacer.

octahedral ligand geometry. A number of three-dimensional structures have been determined by nuclear magnetic resonance (NMR) of the monomer, the dimer,[15,16] and the hexamer[17] and by X-ray crystallography.[18,19] The eight N-terminal residues of the B-chain can be in either an extended conformation or an α-helical conformation that allows the hexamer to adopt three different conformations. Because of the allosteric nature of the transitions among these states,[20] they have been termed T_6, T_3R_3, and R_6, with T and R designating the extended and helical conformations, respectively. NMR and crystallographic studies have established that the structure of the insulin monomer and dimer[15,16,21] in solution adopts the T conformation.

The transition between the allosteric states of the hexamer is mediated via binding of ligands to two classes of binding sites. First, phenolic ligands such as phenol, resorcinol, and cresol bind hydrophobic pockets in the interface between two adjacent dimers in the vicinity of the Cys A6–Cys A11 disulfide bridge. The phenolic hydroxyl group of the ligand forms a hydrogen bond to the carbonyl and the NH group of Cys A6 and Cys A11, respectively. Three binding pockets for phenolic ligands are present in the R_3 trimeric unit, and hence, the T_3R_3 and R_6 conformations bind three and six phenol ligands, respectively. Second, a monovalent anion (e.g., Cl^-, SCN^-, benzoate, or acetate) binds as the fourth ligand in the tetrahedral site around zinc coordinated to His B10.[22] In the absence of any ligands except zinc, the T_3 trimeric unit is favored, whereas the R_3 trimeric unit is dramatically stabilized upon binding of a combination of phenolic ligands and monovalent anions.[23] The allosteric property of the insulin hexamer and the ligand binding has been studied in great detail and can be described in terms of the model of Seydoux, Malhotra, and Bernhard (SMB model),[14,24] which proposes that the T and R conformations of the insulin hexamer will give rise to different classes of binding sites on the T_3 trimeric unit and the R_3 trimeric unit of the hexamer. Moreover, the SMB model predicts an extreme case in which binding of ligand to one R_3 trimeric unit may exclude binding to the opposite trimeric unit of the hexamer, a condition termed half-site reactivity.[25,26]

Depending on the addition of ligands, IDeg will form dihexamers and multihexamers in the formulation and at the injection depot, respectively.[13] In this work, we have applied a range of methods, including X-ray crystallography, small-angle X-ray scattering, circular dichroism spectroscopy, size exclusion chromatography, analytical ultracentrifugation, and transmission electron microscopy, to create a comprehensive picture of the structure, species distribution, ligand binding, conformational states, and morphology of IDeg and to understand the quaternary structures of IDeg in the context of the insulin hexamer being an allosteric protein.

MATERIALS AND METHODS

Materials. Novo Nordisk A/S provided des(B30) human insulin. IDeg was prepared as described in ref 13. The concentration of insulin stock solutions was determined by UV spectroscopy using an E_{276} of 6200 M^{-1} cm^{-1}. All concentrations of human insulin and IDeg refer throughout the text to the nominal concentration of monomeric human insulin and IDeg. Zn^{2+} was added as zinc acetate. All chemicals used were of analytical grade.

Crystal Structure Determination. IDeg and its complexes were crystallized by the hanging drop or microbatch method (see Table 1). Typically, crystals grew within a few days. For cryoprotection, crystals were transferred to a solution containing 0.8 μL of the respective reservoir solution and 0.2 μL of ethylene glycol and immediately flash-frozen at 100 K. Data were collected at different sources and processed using standard programs[27,28] (see Table 1 for details and data statistics). All structures were determined by molecular replacement and refined using the CCP4 or Phenix software suite.[29,30] Details of structure solution are summarized in Table 1.

Size Exclusion Chromatography. SEC was conducted essentially as described previously[8] using a Superose 12 10/30 GL column with a running buffer consisting of 140 mM NaCl, 10 mM Tris-HCl, and 2.0 mM phenol (pH 7.7) or 140 mM NaCl, 10 mM Tris-HCl, and 2.0 mM resorcinol (pH 7.7). Chromatography was conducted at room temperature with an injection volume that was 0.4% of the column volume using a flow of 30 min/column volume (0.8 mL/min).

Analytical Ultracentrifugation. AUC experiments were performed with a BeckmanCoulter (Indianapolis, IN) XL-I

dx.doi.org/10.1021/bi3008609 | *Biochemistry* 2013, 52, 295–309

Table 1. Crystallographic Data

	dimer	T_3R_3	R_6 rhombohedral crystal	R_6 monoclinic crystal
crystallization conditions	4.9 mg/mL IDeg in 0.05 M Hepes (pH 7.8)	4 mg/mL IDeg, 3 zincs/hexamer		5.4 mg/mL IDeg, 0.02 M resorcinol, 0.6 mM zinc acetate
protein solution		5 mM phenol	4 mg/mL IDeg, 3 zincs/ hexamer, 5 mM phenol	
reservoir solution	0.2 M $LiSO_4$, 0.1 M Tris (pH 8.5), 25% (v/v) PEG 3350	0.4 M NaCl, 6% (v/v) ethanol, 100 mM Hepes (pH 7.5)	0.4 M NaCl, 6% (v/v) ethanol, 100 mM Hepes (pH 7.5)	0.6 M imidazole/malonic acid (pH 7.0)
crystallization method	vapor diffusion	microbatch	vapor diffusion	vapor diffusion
PDB entry	4AK0	4AJZ	4AKJ	4AJX
		Data Collection		
wavelength (Å)	1.5418	1.0000	1.5418	1.0000
beamline	N/A	MaxLab 911-3	N/A	SLS X06SA
space group	$I2_13$	$R3$	$R3$	$P2_1$
cell constants				
a, b, c (Å)	77.80, 77.80, 77.80	79.55, 79.55, 38.97	78.717, 78.717, 40.551,	47.31, 62.49, 57.27
α, β, γ (deg)	90, 90, 90	90.000, 90.000, 120.000	90.00, 90.00, 120.00	90.0, 111.8, 90.0
no. of insulin molecules per asymmetric unit	1	2	2	6
biological assembly in the crystal	dimer	hexamer	hexamer	hexamer
resolution range (Å)	55−2.28 (2.42−2.28)	33.93−1.80 (1.85−1.80)	39.34−2.00 (2.03−2.00)	99−1.20 (1.23−1.20)
no. of observations	43182 (7345)	18671 (522)	24285 (614)	381957 (11622)
no. of unique observations	3406 (578)	7500 (342)	6176 (246)	90996 (4311)
completeness (%)	91.9 (100)	87.9 (52.6)	97.5 (75.7)	93.9 (60.5)
R_{sym} (%)	11.6 (37.5)	4.3 (38.6)	3.8 (30.8)	3.8 (36.1)
$I/\sigma(I)$	18.4 (7.1)	14.7 (2.4)	17.0 (1.9)	17.5 (2.8)
		Refinement		
resolution (Å)	55−2.28 (2.34−2.28)	33.9−1.8 (1.85−1.80)	39.3−2.0 (2.06−2.00)	40.5−1.2 (1.22−1.20)
R_{cryst}/R_{free} (%)	16.6/23.2 (16.3/16.2)	18.9/25.5 (24.3/34.7)	19.6/22.9 (31.0/48.7)	14.1/16.0 (20.6/19.6)
no. of reflections (working/test)	3087/314	6819	5890/285	89598/4449
no. of atoms				
total	416	854	883	5212
protein	39224	797	791	4717
ligand		10	42	134
water		47	46	358
ion			4	3
rmsd for bond lengths (Å)	0.018	0.017	0.018	0.014
rmsd for bond angles[a] (deg)	1.802	1.781	1.801	1.614

[a]Root-mean-squared deviation (rmsd) from ideal bond lengths and angles and rmsd of *B* factors of bonded atoms.

analytical ultracentrifuge. Samples were filled in sapphire-capped two- or six-sector Epon centerpieces with a 12 mm optical path length. IDeg was prepared either in 140 mM NaCl and 10 mM Na_2HPO_4/NaH_2PO_4 (pH 7.4) or in 10 mM Tris-HCl (pH 7.6) and 140 mM NaCl with phenol and/or zinc as indicated. Samples were brought to dialysis equilibrium with the solvent either by gel filtration through PD10 columns (GE Healthcare) or by classical dialysis with three buffer exchanges (Slide-A-Lyzer, Pierce). The dialysate was used for dilutions and optical referencing. All experiments were conducted at 20 °C. SV experiments were analyzed with either $c(s)$, the ls(g*) algorithm[8,31] as implemented in SEDFIT version 11.8, or the time-derivative method[32] in DCDT+ version 2.3.1. Single diffusion coefficients of degludec in 140 mM NaCl and 10 mM Na_2HPO_4/NaH_2PO_4 (pH 7.4) were measured by artificial boundary experiments and analyzed with SEDFIT version 11.8. SE experiments were performed at three different speeds, appropriate for the observed molar mass of the system and chosen such that the centrifugal field was varied by a factor of 4. For SE experiments with IDeg and zinc, without phenol, 50 μL of the solution was analyzed at 1500 rpm only. The establishment of the apparent hydrodynamic and thermodynamic equilibrium was ascertained with MATCH. SE data were fit with NONLIN[33] either to a model assuming a single species or, where appropriate, to multiple models of reversible self-association. The best-fit model was selected on the basis of a minimized variance and visual inspection of the residual run pattern. When applicable, confidence limits for the fitted parameters are given in brackets after the best-fit values. The partial specific volume, $\overline{\nu}$, of degludec and the density, ρ, of the buffer were measured with a digital densitometer (model DMA5000M from AntonPaar, Graz, Austria), and the viscosity, η, of the buffer was calculated from the composition using SEDNTERP. Concentrations refer to monomeric IDeg, and values determined by AUC and densitometry refer to the phenol- and zinc-free species.

SAXS. Small-angle X-ray scattering (SAXS) data were collected at the European Molecular Biology Laboratory

(EMBL), beamline X33, on storage ring DORIS of the Deutches Elektronen Synchrotron (DESY, Hamburg, Germany)[34] following standard procedures. Samples contained either IDeg in a concentration range of 0.2−1.4 mM with 3 Zn^{2+}/6Ins, 20 mM resorcinol, 100 mM imidazole, 100 mM NaCl, and 10 mM Tris-HCl (pH 7.5) or IDeg in a concentration range of 0.3−1.3 mM with 5 Zn^{2+}/6Ins, 5 mM phenol, and 10 mM Tris-HCl (pH 7.5). Buffer measurements were taken before and after sample measurements, and the averaged buffer background was subtracted from the sample measurement. Data were recorded during a 4 × 30 s exposure time on a 1M pixel 2D Pilatus detector (DECTRIS) covering a q range pf 0.0067−0.6345 $Å^{-1}$ ($q = 4\pi \sin\theta/\lambda$, where λ is the wavelength and θ is half the scattering angle). Analysis of the individual measurement frames did not reveal any severe radiation damage of the samples during the measurement time. The intensities from the individual scattering curves were truncated and merged to obtain a data file with limited interparticle interference effects. Initial data processing was conducted using programs from the ATSAS package (version 2.4).[35] Background subtractions and Guinier approximations were conducted in PRIMUS.[36] GNOM[37] was used to calculate pair distance distribution function $P(r)$ and to estimate D_{max}. CRYSOL[38] was used to prepare theoretical scattering curves from crystal structures and to fit those to experimental data. DAMMIF[39] was used to calculate ab initio bead models. Individual bead models, 15 in all, were calculated using standard settings. The 15 bead models were subsequently averaged in DAMAVER with normalized spatial discrepancy (NSD) values of 0.765 ± 0.006 (IDeg hexamer) and 0.918675 ± 0.051009 (IDeg dihexamer). OLIGOMER was used to estimate the species distribution in the samples. Form factors based on modeled protein structures were calculated with FFMAKER (Atsas package). The form factors were generated on the basis of the crystal structures of Protein Data Bank (PDB) entries 1EV3 (R_6 hexamer), 1TRZ (T_3R_3 hexamer), and 1MSO (T_6 hexamer). Whenever needed, appropriate crystallographic symmetry operations were applied to construct hexamers (by application of the crystallographic 3-fold rotation symmetry) and dihexamers (by application of a translational symmetry along the z axis of the crystal lattice) in Pymol.[40] This program was also used to generate bead model illustrations.

Circular Dichroism Spectroscopy. CD spectral data were recorded as described in ref 7 except that a Jasco J-815 instrument was used.

Transmission Electron Microscopy. Samples of IDeg at a concentration of 0.41 mM, containing 5 Zn^{2+}/6Ins, were placed on Formvar-coated copper grids, stained with a 2.5% (m/v) uranyl acetate solution, and examined with a FEI Morgagni 268 electron microscope, operating at 80 kV.

RESULTS

Zinc-Free IDeg. *X-ray Crystallography.* The crystal structure of IDeg in its dimeric form was determined at a resolution of 2.3 Å (see Table 1). The crystals belonged to cubic space group $I2_13$, like human and porcine insulin. The structure of IDeg in the cubic crystals shows that insulin is in the T conformation and that the fold is unchanged from human or porcine insulin in the same crystal lattice [e.g., root-mean-square deviation (rmsd) of 47 superposed Cα atoms of 0.24 Å] when compared to wwPDB[41] entry 1B2F.[42] Most importantly, the acyl chain covalently linked to Lys B29 was found to be disordered and not visible in the electron density.

Analytical Ultracentrifugation. To assess the self-association properties of zinc-free IDeg, we performed analytical ultracentrifugation (AUC) experiments. Sedimentation velocity experiments (SV) on a series of different concentrations of IDeg and HI (0.02−0.32 mM) displayed slightly increasing average sedimentation coefficients with increasing concentrations (not shown). Extrapolation of the reciprocal sedimentation coefficients to infinite dilution[43] and correction to standard conditions[44] resulted in $s^0_{20,w}$ values of 0.98 S for IDeg and 0.91 S for HI (see the Supporting Information). The corresponding diffusion coefficients were independently measured in artificial boundary experiments:[45] $D^0_{20,w}$ = 14.8 and 14.3 cm^2/s for IDeg and HI, respectively. In combination with the measured $\bar{v}$ of 0.742 mL/g, these values result in a molar mass of 6.34 kg/mol for the smallest species of IDeg in solution, in agreement with the expected value for the monomer of 6.104 kg/mol. The analogous procedure for human insulin yields a molar mass of 5.93 kg/mol (sequence molar mass of 5.808 kg/mol). Sedimentation equilibrium (SE) gradients of IDeg observed at different rotational speeds were best described by a monomer−dimer−hexamer equilibrium, with a fitted molar mass of 6.23 (6.12−6.34) kg/mol and values for K_{D1-2} of 8.7 (9.7−7.8) × 10^{-4} M and K_{D1-6} of 1.3 (1.6−1.1) × 10^{-17} M (see the Supporting Information). Fixing the molar mass parameter to the expected value resulted in a statistically equivalent fit with slightly shifted values for K_{D1-2} and K_{D1-6}. This is considerably lower than that for wild-type insulins determined previously.[46−48] This finding is confirmed by one-dimensional (1D) ^{1}H NMR dilution series of IDeg and HI (see the Supporting Information).

Crystal Structures of IDeg in Complex with Zinc and Phenolic Ligands. *X-ray Crystallography.* Crystals of IDeg could be obtained in the presence of zinc and phenol, or resorcinol (see Table 1). Despite intense attempts, we did not succeed in crystallizing IDeg in the presence of zinc alone.

When complexed with zinc and a phenolic ligand, IDeg could be crystallized in the T_3R_3 conformation (in a rhombohedral crystal form) or in the R_6 conformation (in both a rhombohedral and a monoclinic crystal form). The structure of the T_3R_3 crystal is unique in that IDeg was found to be in the T_3R_3 conformation although its cell constants are closer to those of insulin in the R_6 conformation in the rhombohedral lattice (Table 1). Consequently, an R_6 insulin structure (PDB entry 1EV3[49]) was used as a starting model for molecular replacement. The structure could be determined easily but was found to be unambiguously in the T_3R_3 conformation with three B-chain termini in the extended conformation and three phenol molecules bound to the IDeg molecules in the R conformation. We envision that initially crystals of R_6 hexamers are formed and subsequently evaporation of phenol from the crystallization drop (and the crystals) triggers a rearrangement of the hexamer from the R_6 to the T_3R_3 conformation. Such interconversion of the T and R states has previously been observed in the rhombohedral crystals.[50,51] The refined structure resembles closely the structure of porcine insulin in complex with phenol (wwPDB entry 1MPJ),[52] with an rmsd of 0.34 Å (based on 84 superposed Cα atoms). The fatty diacid modifications are disordered and cannot be seen in the electron density. In solution in the presence of zinc and phenol the preferred species is dihexamers in R_3T_3−T_3R_3 state (vide infra); however, in the crystal, no dihexameric assembly can be

identified. This is most likely an artifact imposed by the crystal lattice, so that the change in quaternary structure (form hexamer to dihexamer), which is observed in solution, cannot take place in the rhombohedral crystals.

Crystals of IDeg in the R_6 conformation were obtained in two different crystal forms, one in the presence of phenol, ethanol, and NaCl (rhombohedral crystal) and the other in the presence of resorcinol and imidazole (monoclinic crystal). Their structures were determined at resolutions of 2.0 and 1.2 Å, respectively. The crystallization conditions for the rhombohedral crystals were similar to those used to obtain the T_3R_3 crystals; however, the microbatch[53] method was used for crystallization, so that the phenol concentration remained constant during the crystallization experiment. In the R_6 hexamer, both zinc atoms are coordinated by His B10 and an additional chloride ion, similar to the rhombohedral insulin phenol structure (porcine, wwPDB entry 1ZNJ). The fatty diacyl chain attached to Lys B29 was visible for one of the two insulin molecules in the asymmetric unit of the crystal. After generation of the complete hexamer by application of the appropriate crystallographic symmetry, the fatty diacids for one half-site are well-defined and disordered for the other. The fatty diacid is located along the surface of the hexamer where it extends from chain B to cover chain A of this insulin monomer and at the same time occupies a hydrophobic cleft on a neighboring hexamer in the crystal (Figure 2). For this B29-linked fatty diacid, the electron density is weaker for the five ω to $\omega - 5$ carbons of the fatty diacid that are solvent accessible. The binding cleft is located at a dimer–dimer interface within one hexamer and has been shown to bind phenolic ligands upon movement of the A14 tyrosine side chains. On the bottom of this cleft, Leu 13 residues of two A-chains are in contact with the fatty diacid moiety and the side chains of Tyr A14 cover the fatty residues, so that part of the fatty diacid modification at B29 is completely embedded in the protein. Tyr A14 in turn hydrogen bonds via its hydroxyl group to the carbonyl oxygen of the γ-glutamic acid of the B29-linked modification. Additional hydrogen bonding interactions from the main chain carbonyl of Val B18 to the amide nitrogen of the γ-glutamic acid and from the two γ-glutamic acid carboxylic oxygens to the amide nitrogens of Gly B20 and Glu B21 (Figure 2) are observed.

In the monoclinic crystal form (which contains one complete insulin hexamer in the asymmetric unit), two different conformations of the fatty diacid groups were clearly visible in the electron density. One extends from Lys 29 of chain H through the narrow tunnel formed by the B-chain helices (mostly chains H and D) to one zinc atom where one terminal carboxyl oxygen coordinates to the zinc (monodentate coordination) (Figure 2B). Hence, zinc is coordinated in a tetrahedral ligand field by three His B10 side chains and the fatty diacid moiety. The hydrophobic region of this fatty diacid is completely moved out of the solvent and buried in the interior of the hexamer. Contacts are mainly made to Asn 3, Leu 6, and His 10 of the B-chains, which are all on the same face of the helix when insulin is in the R conformation. The more hydrophilic γ-glutamic acid linker is solvent-exposed and also considerably more flexible as there is no well-defined electron density for this part of the fatty diacid chain and the Lys B29 side chain to which it is attached. However, there is convincing electron density for the main chain part of Lys B29, and remarkably, the preceding proline, B28, is found to be in the cis conformation. Interestingly, the fatty diacid interaction is

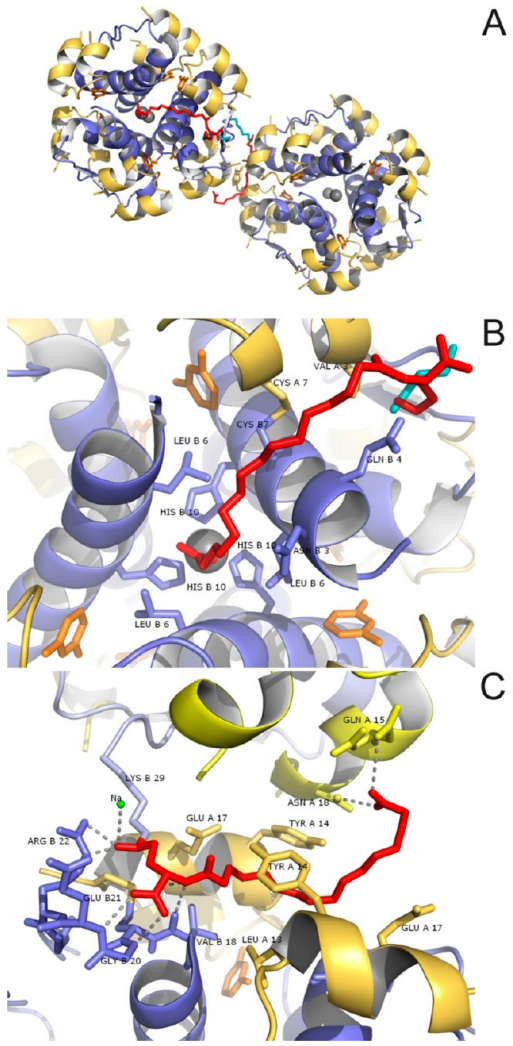

Figure 2. Crystal structure of IDeg in complex with zinc and phenolic ligands. (A) Location of the B29-linked fatty diacid on the IDeg hexamer in the monoclinic crystal involving a neighboring insulin hexamer in the crystal. The two neighboring insulin hexamers are drawn as cartoons with A-chains colored yellow and B-chains blue. Zinc is depicted as gray spheres, and resorcinol molecules are colored orange. The fatty diacid moieties are colored red, and the Lys B29 side chain to which the fatty diacids are covalently attached is colored cyan. (B) Fatty diacid 1, the fatty diacid moiety that coordinates to the structural zinc atom. Side chains that are in the vicinity of 3.5 Å of the fatty diacid are depicted as sticks. The coloring is similar to that of panel A. (C) Fatty diacid 2, which is common for the rhombohedral form. The monoclinic crystal binds to a hydrophobic area on a neighboring hexamer. Side chains within 3.5 Å of the fatty diacid are shown as sticks. Hydrogen bonds or polar contacts are indicated as dashed lines.

seen at only one zinc site, and the second zinc is coordinated by imidazole, of which there is a large excess in the crystallization buffer. As is the case for the fatty diacid coordinating to the first zinc, imidazole is bound in one well-defined conformation, and not disordered as the 3-fold symmetry of the hexamer would suggest.

The second visible B29-linked fatty diacid is bound in the same location as described above for the rhombohedral crystals. In the rhombohedral and monoclinic crystal lattices, hexamers of insulin are arranged in the same way.[49]

dx.doi.org/10.1021/bi3008609 | *Biochemistry* 2013, 52, 295–309

IDeg Structures in the Presence of Zinc and Phenol. *Size Exclusion Chromatography.* On the basis of size exclusion chromatography (SEC), we recently reported that IDeg in a pharmaceutical formulation comprising 0.6 mM IDeg, 0.6 mM zinc acetate, 16 mM *m*-cresol, and 16 mM phenol (pH 7.4) formed dihexamers.[13] To further explore the properties of IDeg with respect to ligand-induced self-association, we studied the species distribution and its dependency on zinc concentration. Chromatograms and the resulting zinc-dependent species distribution of IDeg in the presence of phenol are shown in Figure 3. Increasing the zinc concentration caused the

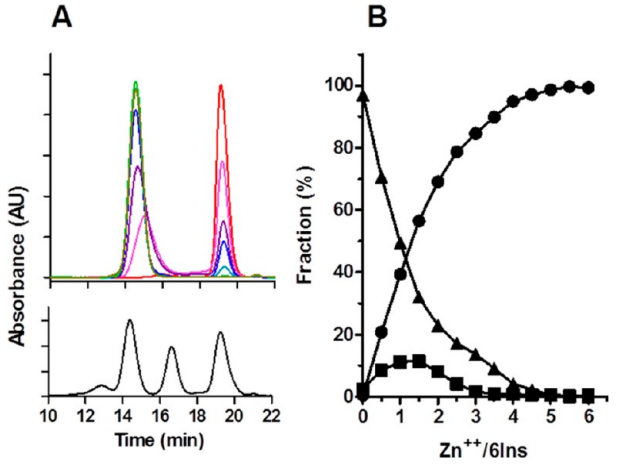

Figure 3. Size distribution of IDeg in the presence of phenol. (A) Chromatograms of SEC runs of 0.6 mM IDeg and 30 mM phenol (pH 7.4) and zinc ratio in integers from 0–6 Zn^{2+}/6Ins indicated by different colors (red, pink, purple, blue, cyan, green, and olive). In black is shown the chromatogram of the molecular mass standards (HSA dimer, HSA, covalent insulin hexamer, and monomeric insulin at 13.0, 14.4, 16.4, and 18.3 min, respectively). (B) Species distribution obtained via SEC after integration indicated by triangles (monomer), squares (intermediate), and circles (dihexamer).

magnitude of a peak at 19.3 min (corresponding to zinc-free monomeric IDeg) to diminish gradually and concomitantly a distinct peak to appear at 14.5 min close to the 66 kDa standard. At a zinc ratio of 5–6 Zn^{2+}/6Ins, the 14.5 min component takes up 100% of the integrated area. On the basis of the molecular mass standards, this peak is tentatively assigned to the dihexamer of IDeg. For 1–2 Zn^{2+}/6Ins, a minor chromatographically unresolved component was also observed.

Analytical Ultracentrifugation. To confirm the assignment of the predominant species in the presence of zinc and phenol to a dihexamer of IDeg, SV experiments were performed at different concentrations (0.6–0.01 mM) of IDeg containing 5 Zn^{2+}/6Ins and 30 mM phenol. These displayed essentially a single sedimenting species and no indications of further self-association. Extrapolation to infinite dilution (not shown) and corrections to standard conditions resulted in an $s^0_{20,w}$ of 5.3 S. Samples with <0.2 mM IDeg, which had an average sedimentation coefficient close to that at infinite dilution, were also evaluated with the time derivative method to simultaneously determine s and D and therefrom the molar mass.[32] An average molar mass of 76.6 ± 3.2 kg/mol (n = 5) was thus determined (Figure 4A). SE experiments over the same concentration range yielded a molar mass at infinite dilution of 80.5 kg/mol (not shown). These results are in agreement with the species sedimenting at 5.3 S being a dihexamer of IDeg.

Small-Angle X-ray Scattering. X-ray scattering data were collected at four different concentrations of IDeg ranging from 0.2 to 1.4 mM with 5 Zn^{2+}/6Ins and 5 mM phenol. Interparticle interactions could be observed at high concentrations but were weakened at the lower concentrations. The individual scattering curves superposed well, indicating that the molecular shape and state of self-association were unchanged within the concentration range analyzed. Using the Guinier approximation, the radius of gyration, R_g, was estimated to be 2.8 ± 0.03 nm. A pair distance distribution function, $P(r)$, was calculated by an indirect Fourier transformation of a merged data set where the effects of interparticle interference were reduced (Figure 4B). From the $P(r)$ plot, the maximal length found within the particle, D_{max}, was determined to be 8.0 nm. The $P(r)$ data were used to calculate low-resolution ab initio models using DAMMIF. This software generates reconstructions of the protein shape by making assemblies of densely packed beads. DAMMIF was used to generate a number of independent models of the protein shape that subsequently were averaged to gain a representation of the most typical one. An averaged and filtered bead model is shown in Figure 4B. The overall shape of the model bears a strong resemblance to an expected dihexameric insulin structure.

IDeg Structures in the Presence of Zinc and Resorcinol. *Size Exclusion Chromatography.* Resorcinol, NaCl, and imidazole are known to stabilize the R_6 structure of HI,[23,54] and hence, the effect of these ligands on the zinc-dependent self-association of IDeg was studied. When phenol was substituted for resorcinol (Figure 5A), an additional distinct peak is observed at 15.6 min with ∼80% of the total area at 2 Zn^{2+}/6Ins. A further increase in the level of zinc causes the disappearance of this species and the appearance of a peak with a position and a width similar to those assigned to the dihexamer (Figure 3). In the presence of 150 mM NaCl (Figure 5B), an even more distinct transition between these three species is observed with 100% of the 15.6 min species at 2 Zn^{2+}/6Ins. The 15.6 min species does not coincide with the SEC standard of the insulin hexamer; however, the findings that this species is prominent at a defined stoichiometry of 2 Zn^{2+}/6Ins and that it is favored in the presence of resorcinol relative to phenol suggest that the peak represents a hexamer of IDeg. To interlink to the buffer conditions that resulted in a crystal structure (Figure 2), the combined effect of imidazole and resorcinol was tested (Figure 5C). Again, the monomer is virtually absent above 2 Zn^{2+}/6Ins and replaced by the presumed hexamer. However, when the zinc ratio was further increased, only ∼40% of the presumed dihexamer species was formed. Thus, imidazole seems to suppress the formation of the IDeg dihexamer.

Small-Angle X-ray Scattering. To further analyze the presumptive hexameric species deducted from the SEC data, a SAXS analysis was conducted on samples containing IDeg in a concentration range from 0.2 to 1.4 mM, with 3 Zn^{2+}/6Ins, 20 mM resorcinol, 100 mM imidazole, and 100 mM NaCl. From the scattering curve and $P(r)$ plot in Figure 6, R_g (2.0 nm) and D_{max} (5.2 nm) were deduced. The dimensions were clearly smaller than those observed for the dihexamer (Figure 4). The bell-shaped $P(r)$ curve together with the R_g and D_{max} dimensions indicates a nearly spherical structure, as would be expected from a hexameric insulin assembly. Ab initio bead models were calculated with DAMMIF. The dimensions and

dx.doi.org/10.1021/bi3008609 | *Biochemistry* 2013, 52, 295–309

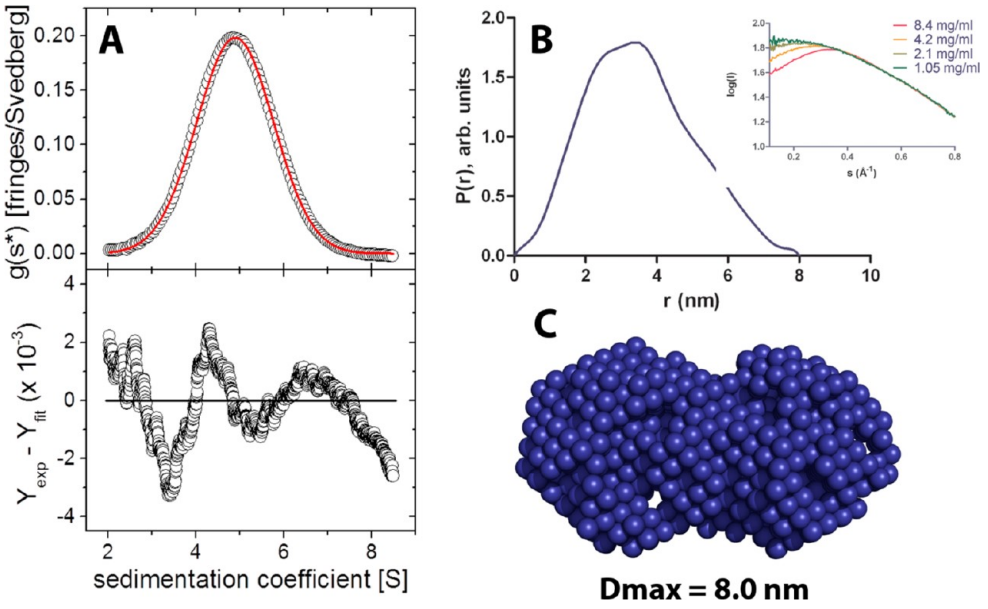

Figure 4. AUC and SAXS of IDeg in the presence of zinc and phenol. (A) AUC of 0.19 μM IDeg, 5 Zn^{2+}/6Ins, and 30 mM phenol (pH 7.4) depicted as a $g(s^*)$ curve (top, open circles); only every 10th data point is shown. The red line represents simulated data for a single sedimenting species with an s of 4.94 S, a D^* of 6.31 × 10^{-7} cm^2/s, and an M_w of 75.1 kg/mol. The deviations between the experimental and simulated data are displayed (bottom); every data point is shown, with an overall rmsd of 1.19 mFringes. (B) SAXS of IDeg with 5 Zn^{2+}/6Ins and 5 mM phenol (pH 7.5) depicted as a pair distance distribution plot, $P(r)$. From the plot, D_{max} was determined to be 8.0 nm. The inset shows the experimental SAXS data and the concentration-dependent intensity decrease at low values of r, caused by interparticle interference at high concentrations. (C) SAXS model based on the data presented in panel B. The model is an averaged and filtered ab initio bead model calculated with DAMMIF.

spherical shape of the averaged DAMMIF model shown in Figure 6 resemble a hexameric insulin structure. A comparison with a simulated scattering curve calculated from the crystal structure of IDeg in the monoclinic crystal form, determined in this study, is also shown in Figure 6. There is a good overall fit (χ^2 = 0.988) indicating that IDeg is a hexamer under these sample conditions.

Conformational States of IDeg in the Presence of Zinc and a Phenolic Ligand. *Near-UV Circular Dichroism Spectroscopy*. Previously, the ellipticity at 251 nm of zinc-bound insulin was found to be proportional to the extent of conformational change from T_6 via T_3R_3 to R_6 conformation.[20,55] To relate the species distribution (Figure 5) to insulin conformation, we studied the dependency of the ellipticity on the zinc ratio at saturating phenolic ligand conditions with HI as a reference. First, we established the amplitude change of the ellipticity at 251 nm related to the formation of R_6 hexamers of HI. In the presence of chloride or imidazole, the amplitude changed from −1.8 to −8.0 M^{-1} cm^{-1} upon titration of zinc (Figure 7A). Via titration in the presence of phenol in the absence of NaCl, the amplitude saturates at around −5 M^{-1} cm^{-1}, indicating the formation of the intermediate state, T_3R_3. When phenol was replaced with resorcinol, a similar change in amplitude and saturation at 2 Zn^{2+}/6Ins is observed except that saturation at −8.0 M^{-1} cm^{-1} is reached even in the absence of NaCl (see the Supporting Information). These results with human insulin are in accordance with literature data. Given (Figure 2) that the structural features of the phenolic binding pockets of IDeg are very similar to those of human insulin, we can assume that for IDeg the amplitude change from approximately −2.0 to −8.0 M^{-1} cm^{-1} represents a conformational change from the T_6 state to the R_6 state and that intermediate intensities denote combinations of T and R states.

The conformational change of IDeg as a function of zinc is displayed in Figure 7B. Titration in the presence of phenol but in the absence of added ligands for the His B10 site results in a shallow saturation curve leveling off at 3−4 Zn^{2+}/6Ins and at an intensity of −5.0 M^{-1} cm^{-1}. In the presence of NaCl or imidazole, the curves decline more steeply until ∼2 Zn^{2+}/6Ins at an intensity of −6.8 M^{-1} cm^{-1} but revert to a plateau at −5.0 M^{-1} cm^{-1} for ratios of >4 Zn^{2+}/6Ins. On the basis of the change in amplitude for HI presented here (Figure 7A), the data suggest that in the presence of phenol, IDeg with 4−6 Zn^{2+}/6Ins adopts a mixed T−R state. Furthermore, at intermediate zinc ratios (2−3 Zn^{2+}/6Ins) in the presence of NaCl or imidazole, the distribution of conformations is shifted slightly toward a larger population of R states, however, without saturation.

When phenol was exchanged for resorcinol (Figure 7C), increasing the zinc ratio led to a minimum in ellipticity at ∼2 Zn^{2+}/6Ins at an intensity of −7.5 M^{-1} cm^{-1}, but with a further increase in the level of zinc, the amplitude gradually reverts to −5 M^{-1} cm^{-1}. In the presence of NaCl, the nonmonotonous curve shape becomes even more pronounced with a sharp turning point at 2 Zn^{2+}/6Ins and an amplitude of −8.7 M^{-1} cm^{-1}. This suggests that in the presence of resorcinol and 2 Zn^{2+}/6Ins the R state is favored but that additional zinc drives the equilibrium to a mixed T and R state. The presence of imidazole results in a similar saturation at 2 Zn^{2+}/6Ins and −8.3 M^{-1} cm^{-1}, but in contrast to NaCl, imidazole appears to stabilize the R conformation also at higher zinc ratios. The data suggest that the presence of resorcinol allows IDeg to adopt an R_6 state under conditions of 2 Zn^{2+}/6Ins but also at higher zinc ratios if imidazole is present.

Via comparison of the data presented in Figures 5 and 7, it is evident that the levels of the hexamer and dihexamer coincide with ellipticities of approximately −8.0 and −5.0 M^{-1} cm^{-1},

dx.doi.org/10.1021/bi3008609 | *Biochemistry* 2013, 52, 295−309

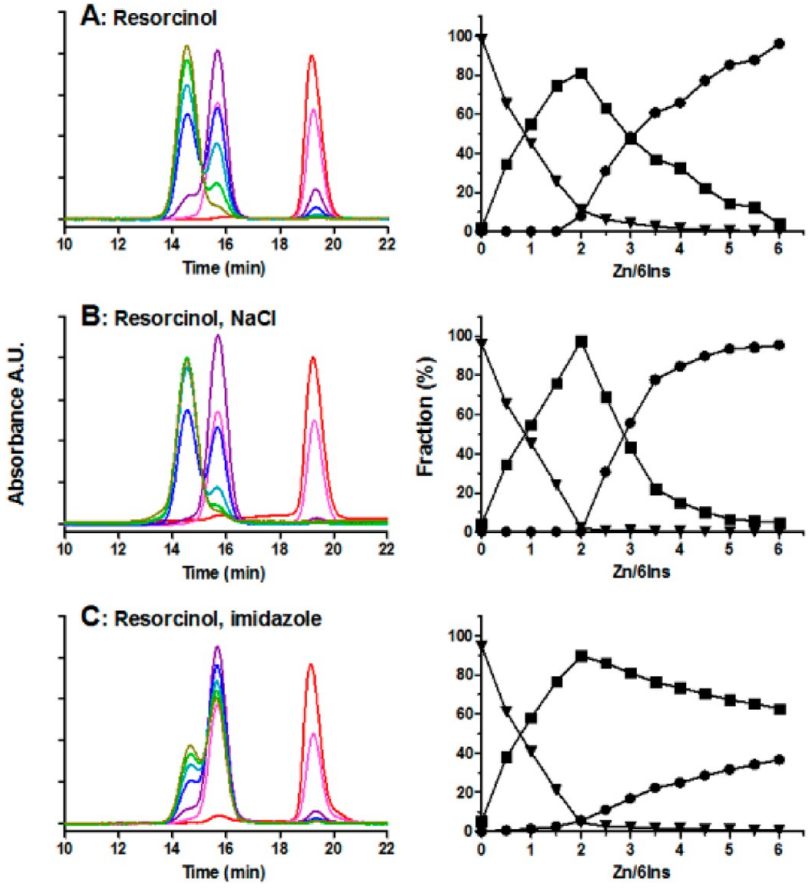

Figure 5. Size distribution of IDeg in the presence of Zn^{2+}, resorcinol, NaCl, and imidazole. Chromatograms (left) and species distribution (right) of IDeg in the presence of Zn^{2+}, resorcinol, NaCl, and imidazole. The zinc ratios varied in integers from 0–6 Zn^{2+}/6Ins and are depicted in various colors (red, pink, purple, blue, cyan, green, and olive), and the species distribution obtained from the SEC after integration is indicated by triangles (monomer), squares (presumed hexamer), and circles (dihexamer). The molecular mass standards (not shown) were similar to those depicted in Figure 3. (A) Samples of 0.6 mM IDeg and 30 mM resorcinol (pH 7.4). (B) Samples of 0.6 mM IDeg, 150 mM NaCl, and 30 mM resorcinol (pH 7.4). (C) Samples of 0.6 mM IDeg, 100 mM imidazole, and 30 mM resorcinol (pH 7.4).

respectively. It was possible to simulate the data (see the Supporting Information) in panels B and C of Figure 7 by using the species distribution presented in Figures 3 and 5. Because of the linkage between the quaternary state and the conformational state, we conclude that the observed IDeg hexamer adopts an R_6 conformation whereas the IDeg dihexamer appears in a combination of T and R states.

Structural Modeling of the Dihexamer Conformation. To further elucidate the structural organization of the dihexamer, we compared the experimental X-ray scattering data to a reconstruction of insulin dihexamer assemblies in different allosteric states. On the basis of the near-UV circular dichroism measurements, where the structural conformation of the dihexamer was found to be a combination of T and R states, the following structural models of the dihexamer were prepared: (1) T_3R_3–T_3R_3, (2) R_3T_3–T_3R_3, and (3) T_3R_3–R_3T_3. The models assume an equal distribution of T and R states within the dihexamer and an overall symmetric dihexamer but with a nonsymmetric hexamer unit. For the sake of simplicity, we have excluded the model on the basis of symmetric hexamer units, i.e., a combination of 50% T_3T_3–T_3T_3 and 50% R_3R_3–R_3R_3, which can be ruled out as viable model (see Discussion). For comparison, two other models were prepared to have two extreme cases, T_3T_3–T_3T_3 and R_3R_3–R_3R_3, where the allosteric state is either all T or all R. The maximal length found within the dihexamer was from the pair distance distribution function determined to 8.0 nm. An insulin hexamer in a T_6 conformation has a cylinder-shaped structure with a diameter of ~4.7 nm and a height of ~3.4 nm. The hexamer shape in the R_6 state is more spherical, with one edge being longer, ~4.8 nm, while the short side measures ~4.0 nm. The shortest distance is along the 3-fold symmetry axis through the two Zn^{2+} ions. To fulfill the requirement of a total length of 8.0 nm (Figure 4), a hexamer–hexamer interaction with the symmetry 3-fold axis of each hexamer pointing toward each other is needed. Therefore, the structural models were generated with this motif. Calculated scattering curves based on the generated structural models are depicted in Figure 8 together with the fit to the experimental data. As one can see in Figure 8, the theoretical scattering curves differ markedly and are sensitive to the allosteric states of the individual hexamers. The difference is most prominent in the region around 0.2 $Å^{-1}$ where the R_3R_3–R_3R_3 dihexamer has a pronounced minimum while the T_3T_3–T_3T_3 dihexamer displays a shallower curve shape. Models with a T_3R_3 composition generated curves between the two. The model with the best fit to experimental data was the R_3T_3–T_3R_3 model. The simulated curve for this dihexamer follows closely the experimental oscillations that indicate that the shape and internal density distribution of the experimental molecule are described well by the structural

dx.doi.org/10.1021/bi3008609 | *Biochemistry* 2013, 52, 295–309

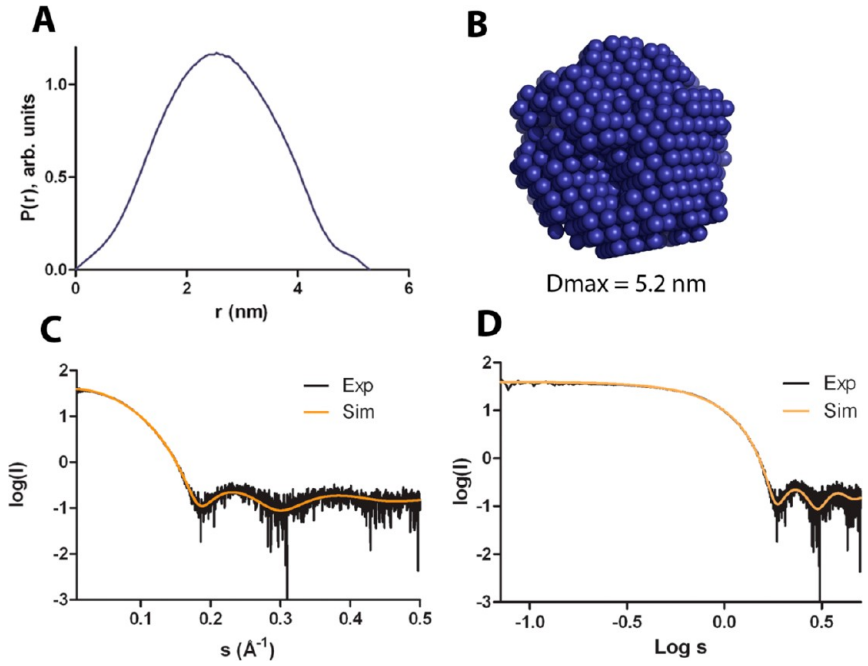

Figure 6. SAXS of IDeg in the presence of zinc, imidazole, and resorcinol. SAXS scattering data of IDeg (0.2−1.4 mM) containing 3 Zn^{2+}/6Ins, 20 mM resorcinol, 100 mM imidazole, 100 mM NaCl, and 10 mM Tris (pH 7.5). (A) Data presented as the pair distance distribution function collected from a sample. (B) An ab initio model calculated by DAMMIF. The spherical character and dimensions of the model resemble those of an insulin hexamer. (C and D) When the hexamer crystal structure was applied for simulation of scattering curves (orange), a very good fit in the high-resolution (C) and low-resolution (D) regions was obtained when compared with the experimental data (black).

model. There was no improvement in the fit upon introduction of other oligomeric species like hexamers, dimers, or monomers.

IDeg Structures in the Absence of Phenol. *Transmission Electron Microscopy.* TEM visualized IDeg, containing 5 Zn^{2+}/6Ins and deprived for phenol as consisting of regular and long strands (Figure 9A) with a mean width of 6.3 ± 0.9 nm (Figure 9B). The hydrated width is likely to be smaller, as the fibers adhere to the grid upon drying and hence appear to be broader. The single strands possess a very high degree of internal order, as a uniform width, and no kinks or other defects were observed for all samples examined. It was not possible to determine an average length, and no aspect ratio is reported. The distribution is very close to Gaussian, which indicates that only a single kind of fiber is present. The visualization by TEM also suggests that individual fibers are entangled and will probably also be in solution. The fibers exhibit a cursory likeness to insulin amyloid fibrils. These amyloid fibrils are characterized by predominance of β-sheet rich secondary structure.[56] However, IDeg displays no evidence of amyloid-type β-sheet structures as evidenced by FTIR (see the Supporting Information).

Analytical Ultracentrifugation. To further characterize the higher-order complexes of IDeg, analytical ultracentrifugation was performed on a formulation of IDeg, containing 5 Zn^{2+}/6Ins and deprived of phenol. In sedimentation velocity, very steep boundaries together with a considerable negative concentration dependence of the average sedimentation coefficient were observed for samples of IDeg containing 5 Zn^{2+}/6Ins. Extrapolation to infinite dilution and correction to standard conditions yielded an $s^0_{20,w}$ of 28.8 S (see the Supporting Information). SE experiments also displayed a remarkable degree of negative concentration dependence of the equilibrium gradient curvature (Figure 10). The average molar mass at infinite dilution (M_0) was 59.7 × 10^3 kg/mol (see the Supporting Information). The maximal, predicted sedimentation coefficient for a particle of the same molar mass is 524 S. The difference between this and the measured value could be a high degree of molecular asymmetry or an extremely high degree of branching, such as that observed for complex carbohydrates.[57] Because of the entanglement of fibers described above (Figure 9), it is unlikely, however, that the measured sedimentation coefficient and molar mass reflect the properties of an ensemble of isolated fibers.

To examine the conformational state of the high-molecular mass complex of IDeg deprived of phenol, we measured the ellipticity at 251 nm of the phenol-deprived zinc complex of IDeg. We found that after removal of phenol the ellipticity changes from −5 to approximately −2 M^{-1} cm^{-1}, corresponding to a conformational change to the T_6 state (see the Supporting Information and Figure 7).

■ DISCUSSION

IDeg is a novel acylated insulin with an ultralong blood glucose lowering effect in humans.[11,12] On the basis of a comprehensive set of data, we have described the structure, the self-association, and the ligand binding properties. These properties provide the basis for the new concept for protraction of insulin based on dihexamer and multihexamer formation.

Zinc-Free Structure. The overall three-dimensional structure of the protein fold of zinc-free IDeg is essentially identical to that of human insulin. No changes in the dimerization interface are observed, although the tendency of IDeg to self-associate in the absence of zinc is weakened by 1 order of magnitude compared to that of HI.[46−48] A similar tendency was observed for a related engineered des30 insulin myristoylated at position B29.[7] In that case, the weakened dimer formation was explained by the myristoyl side chain

dx.doi.org/10.1021/bi3008609 | *Biochemistry* 2013, 52, 295−309

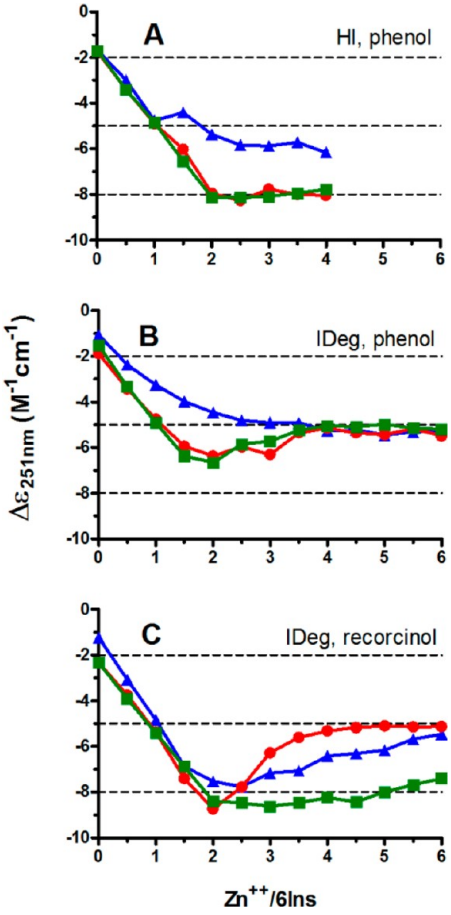

Figure 7. CD spectroscopy probing the conformational change of HI and IDeg. Conformational change as observed by ellipticity at 251 nm as a function of zinc ratio for various conditions of ligands: (A) 0.6 mM human insulin and 30 mM phenol (pH 7.4) (triangles) with the addition of either 150 mM NaCl (circles) or 100 mM imidazole (squares), (B) 0.6 mM IDeg and 30 mM phenol (pH 7.4) (triangles) with the addition of either 150 mM NaCl (circles) or 100 mM imidazole (squares), and (C) 0.6 mM IDeg and 30 mM resorcinol (pH 7.4) (triangles) with the addition of either 150 mM NaCl (circles) or 100 mM imidazole (squares).

being in close contact with the putative dimer interface and thus reducing the likelihood of dimer formation. A similar explanation may very well be applicable for IDeg. This speculation is supported when comparing the $s_0/s^0_{20,w}$ ratio for IDeg and HI as a relative measure of molecular expansion.[58] On the basis of the values determined here, this ratio is found to be 1.29 and 1.17 for human insulin and IDeg, respectively. This means that the monomer of human insulin in solution in a hydrodynamic sense is relatively more expanded than that of IDeg. This is an indication that the diacyl chain of IDeg is collapsed onto the peptide backbone rather than freely accessible to the solvent.

Distinct Zinc Species of IDeg. On the basis of SEC, AUC, and SAXS, a consistent picture of the zinc complexes formed by IDeg in solution has emerged. Depending on the presence of ligands such as zinc, phenolic ligands, and ligands for the His B10 zinc site, IDeg can form hexamers, dihexamers, and multihexamers. The dihexamer is the sole and finite species observed in the presence of phenol and zinc above 3−4 Zn^{2+}/6Ins. A hexamer of IDeg is observed in a fairly narrow space of conditions characterized by ∼2 Zn^{2+}/6Ins and resorcinol and is further stabilized by imidazole. The multihexamers are large linear supramolecular zinc structures of IDeg formed in the absence of phenol. These remarkable structures display an average molar mass (M_0) of 59.7 × 10^3 kg/mol and a width of 6.3 ± 0.9 nm from linear arrays of hundreds of hexamers. The average molar mass of the multihexamer derived from AUC data presented here for IDeg is ∼1 order of magnitude larger than that previously reported by multiangle light scattering-detected SEC that resulted in an average molar mass of 2.9 MDa.[13] This discrepancy may originate in the different sensitivity of the two methods to the entanglement of the fibers or in kinetic aspects of the formation of multihexamers. The time of sampling after removal of phenol is on the order of minutes for multiangle light scattering-detected SEC but hours for SE−AUC. For a related acylated insulin, Lys^{B29}(N^{ε}-heptadecandioyl) des(B30) human insulin, similar long straight rods were found in a SAXS study (DOI 10.1021/bi3008615).

Hexamers, Dihexamers, and Multihexamers of IDeg Are Composed of Protomers of Classical Hexamers. In the following, we will discuss the zinc complexes of IDeg on a structural level and how they compare to those described for HI. The X-ray structures of IDeg crystallized in the presence of zinc and a phenolic ligand show that the protein fold is highly similar to that of human insulin and Lys^{B29}(N^{ε}-tetradecanoyl) des(B30) human insulin[59] in both T and R conformations. This confirms that the allosteric transitions between the R and T conformations are possible and will readily be adopted by the degludec molecule upon addition of, e.g., phenolic ligands at the right concentrations. Upon examination of the fatty diacid modifications, the crystal structures highlight some of the structural properties of the acylation: (1) The fatty diacid group linked to B29 will favorably interact with hydrophobic clefts and tunnels on the protein surface. (2) The fatty diacid can via its carboxy group in the ω position coordinate to zinc, also as an additional ligand to the zinc atoms coordinated by His B10 in the center of the hexamer. (3) As Lys B29 is located at the terminus of the B-chain and its side chain projects toward the solvent, the fatty diacid modification has complete conformational freedom to the extent that it can be completely disordered in the crystal. (4) The attachment of the rather long and bulky moiety at B29 does not influence the folding of the insulin molecule, as shown by crystal structures in dimeric and different hexameric states.

Although we observe an intriguing network of hydrogen bonding and hydrophobic interactions between the B29-linked fatty diacid of one hexamer and a neighboring hexamer in the monoclinic and rhombohedral crystal forms (Figure 2C), we do not believe that this interaction is responsible for the self-association observed in solution but rather is augmented by the tight (and nearly identical) arrangement of hexamers in both crystal lattices based on the following arguments. First, such an association would after application of the crystallographic symmetry lead to infinite polymeric aggregates, and not explain the dimerization of hexamers. Furthermore, it has been shown previously for insulin that the binding site on the neighboring hexamer binds different hydrophobic ligands (ref 51 and references cited therein), and finally, IDeg hexamers in the R_6 conformation have been shown in this work not to associate in dihexamers at concentrations employed for crystallization.

Another interesting aspect of the crystal structures in the R_6 conformation is that in both crystals not all fatty diacid moieties are defined in the electron density; this implies that the presence of the B29-linked fatty diacid induces or amplifies a

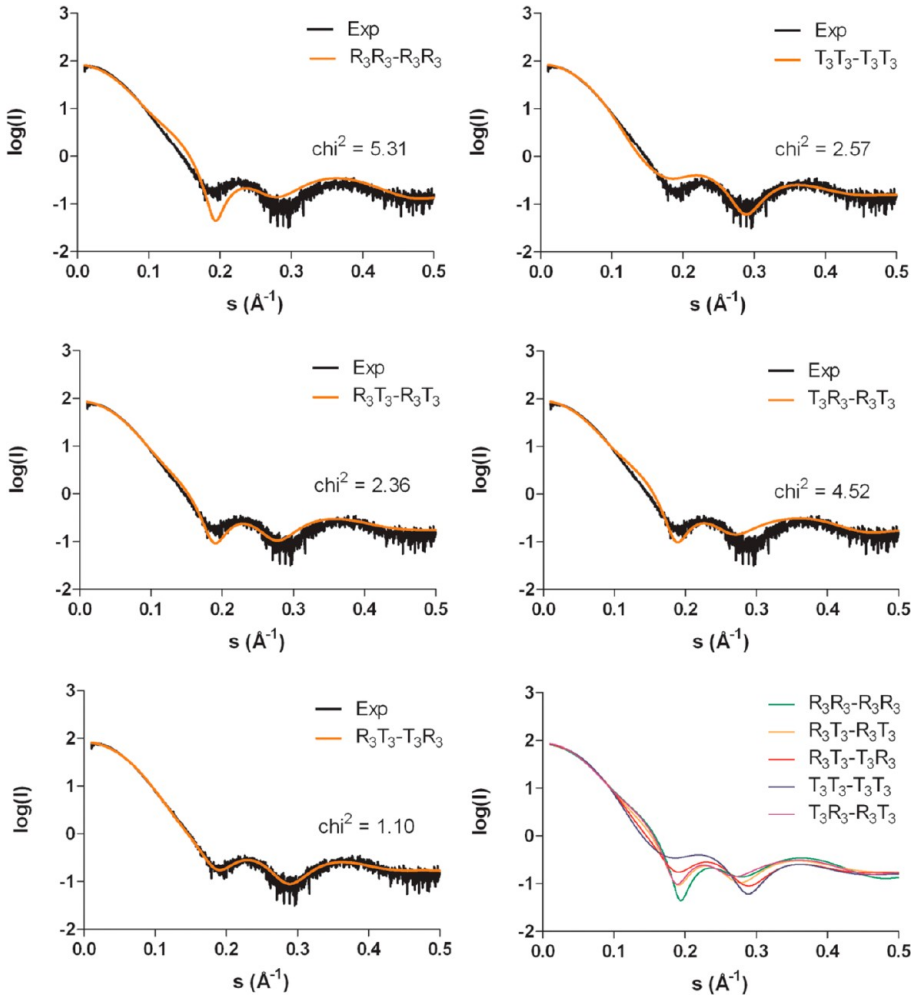

Figure 8. Theoretical scattering curves for various models of dihexamers of IDeg compared with the experimental data. Comparison of theoretical scattering curves (orange lines) with the experimental (black lines). The theoretical curves originate from dihexamer models, based on crystal structures, with variation in the allosteric states of the hexamers. The dihexamer with the R_3T_3–T_3R_3 conformation has the best fit against experimental data (χ^2 = 1.10).

deviation from perfect symmetry within the insulin hexamer, in agreement with what was observed for a related insulin analogue, $Lys^{B29}(N^{\varepsilon}$-tetradecanoyl) des(B30) human insulin.[59]

The dimensions and shapes of the species observed in solutions are in line with the hexamer and dihexamer. Moreover, in the presence of resorcinol, the stoichiometry is 2 mol of zinc/6 mol of degludec of IDeg (Figure 7C). This is in line with the formation of a classical insulin hexamer structure that binds two zinc atoms to each of the His B10 sites. We conclude that the basic building blocks of the dihexamer and the multihexamer are similar to a classical insulin hexamer.

Model for the Conformation of the Dihexamer Derived by Induction. Our data show that there is a tight link between the conformational state and the formation of the quaternary and higher-order structure of IDeg. This is observed as hexamers preferring the R_6 state, dihexamers that prefer an apparent combination of equal shares of T_3 and R_3 trimeric units, and multihexamers adopting an all-T conformation. On the basis of the findings described above, we now induce a structural model for the dihexamer that is predominant in the pharmaceutical formulation.

By a combinatorial approach, the conformational state of the dihexamer population can be imagined to be (1) a mixture of R_3R_3–R_3R_3 and T_3T_3–T_3T_3, (2) R_3R_3–T_3T_3, (3) T_3R_3–T_3R_3, (4) T_3R_3–R_3T_3, or (5) R_3T_3–T_3R_3, where the dashes designate the hexamer–hexamer contact. In line with the concept of assembly of protein quaternary structures by Monod,[60] the hexamer unit can be viewed as a protomer with either symmetric character (T_6 or R_6 state) or asymmetric character (T_3R_3 state). Experimentally, we find dihexamers of IDeg in the presence of phenol as a finite and predominant species. According to Monod, a symmetric protomer would be expected to grow consecutively and infinitely along with addition of effectors of polymerization. Models 1 and 2 cannot explain the observation of a finite and predominant dihexamer and can thus be ruled out. Model 3 does not explain the finding of finite and predominate dihexamers because the T_3R_3–T_3R_3 form should continue polymerization with addition of effectors. Model 4 is not in accordance with the data showing that the conformational transition to the R_6 state is closely linked to dissociation of the dihexamer to the hexamer, a finding that strongly suggests a face-to-face arrangement of the T_3 trimeric unit of a T_3R_6 structure in the dihexamer of IDeg. Furthermore, we find that the multihexamer adopts an all-T state, which implies that the formation of the multihexamer takes place via interactions between the T_3 trimeric units. A dihexamer in the T_3R_3–R_3T_3 conformation (model 4) would moreover suggest easy polymerization of the T_3R_3–R_3T_3 form with another T_3R_3–

dx.doi.org/10.1021/bi3008609 | *Biochemistry* 2013, 52, 295–309

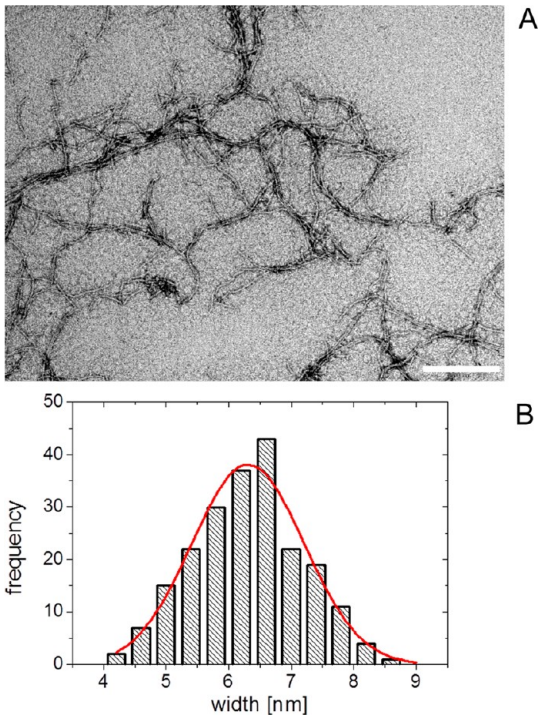

Figure 9. TEM imaging of zinc complexes of IDeg in the absence of a phenolic ligand. (A) Elongated degludec structures of 0.6 mM degludec, 5 Zn^{2+}/6Ins, and 30 mM phenol depleted for phenol on a NAP10 column. The scale bar represents 200 nm. (B) Histogram of measured widths of 213 individual fibers. The red line represents a Gaussian fit to the histogram.

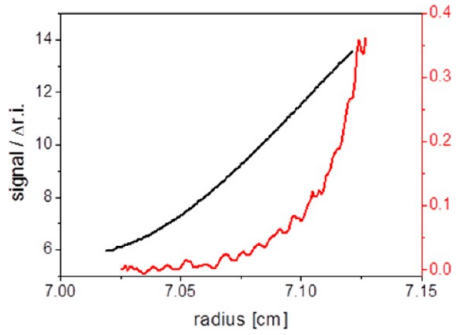

Figure 10. AUC of IDeg containing 5 Zn^{2+}/6Ins and deprived of phenol. AUC–SE curves represent stationary concentration gradients at 1500 rpm of a formulation of IDeg containing 5 Zn^{2+}/6Ins and deprived of phenol on a NAP10 column. The lines represent starting concentrations 0.59 mM (black) and 0.04 mM (red).

R_3T_3 species to form T_3R_3–R_3T_3–T_3R_3–R_3T_3 structures even in the presence of a phenolic ligand. Again this is contradicted by the finding of finite and predominate dihexamers in the presence of phenol. In model 5, the R_3T_3–T_3R_3 conformation for the IDeg dihexamer is the simplest model that is consistent with our data. The R_3T_3–T_3R_3 model that we induced from several lines of experimental evidence is supported by the simulation of SAXS scattering data (Figure 6), from which it is evident that the R_3T_3–T_3R_3 model results in the best fit to the experimental scattering data. A similar conclusion was drawn on the basis of SAXS studies for a related acylated insulin, Lys^{B29}(N^{ε}-heptadecandioyl) des(B30) human insulin (DOI 10.1021/bi3008615).

The R_3T_3–T_3R_3 model also implies the simplest possible mechanism for the formation of linear structures of multihexamers once phenol dissociates from the dihexamer. Hence, when IDeg is deprived of phenol, the conformation changes from the R_3T_3–T_3R_3 structure to the T_3T_3–T_3T_3 structure; then the R_3 trimeric unit is no longer blocking further interaction, and the polymerization to linear multihexamers via a symmetric protomer can proceed. The R_3T_3–T_3R_3 model moreover provides a likely explanation for why the existence of hexamers of IDeg is coupled to the R_6 state. Bloom et al.[26] reported that human insulin in the presence of certain ligands behaves with a half-site reactivity that precludes formation of the R_6 state. It is tempting to interpret the existence of a protomer that favors the R_3T_3 conformation as an extreme case half-site reactivity originating in the interaction of the two protomers of the IDeg dihexamer. This suggests that the structure and allosteric properties of the dihexamer of IDeg are in line with the SMB model. Moreover, it would also suggest that the carboxylic group in the ω position of the B29-linked moiety is capable of stabilizing the R_3 trimeric units of the IDeg dihexamer by serving as a ligand for either the phenol binding pocket or the His B10 zinc site at either the same protomer or more likely the adjacent protomer. Such an interaction could lock the R_3T_3–T_3R_3 structure and lead to half-site reactivity. In this respect, we believe that the phenomenon of dihexamer formation of IDeg is different from the formation of an infinite dihexamer observed for human insulin by Hvidt,[61] Attri et al.,[62] and Phillips and colleagues.[63]

The idea that the carboxylic group in the ω position of the B29-linked moiety serves as a ligand for the phenolic pocket or the His B10 zinc site at the adjacent protomer is supported by our X-ray structure, in which it was shown that the zinc coordinated in the site at His B10 readily accepts the B29-linked fatty diacid as an additional ligand. Interestingly, the fatty diacid in the crystal structure coordinates to zinc in a monodentate fashion. We propose that also in the solution state the carboxylic group in the ω position of the diacyl chain can serve as a ligand for the zinc in the His B10 site. The octahedral coordination of zinc bound to His B10 in the T state will require three external ligands, and we can speculate that these consist of one or more carboxylic groups offered from the B29 attachmets from a neighboring degludec hexamer supplemented with carboxylic residues from the self, or with addition of water. An additional driving force for the formation of the IDeg dihexamer may be binding of zinc ions. A putative role for zinc in IDeg besides coordination to the His B10 site could be that the carboxylic acid of the γ-L-glutamic moiety of adjacent hexamers coordinates one or more shared zinc atoms and in this way stabilizes the structure and neutralizes the negative charge of the γ-L-glutamic acid. The finding of linear higher-order structures suggests a bivalent nature of the interaction between the individual hexamers rather than a polyvalent form that would result in a meshlike structure. The design strategy and structural requirement for the fatty diacid moiety and the linker to form the multihexamer structures have been described previously.[13]

CONCLUSION

The engineered insulin, IDeg, possesses unique properties originating in the B29-linked diacyl group that modulate the inherent allosteric character of the insulin zinc hexamer and consequently result in distinct species in the pharmaceutical formulation and in the subcutaneous depot after injection

(Figure 11). In a formulation comprising zinc and phenol, IDeg is organized as finite dihexamers in the $R_3T_3-T_3R_3$

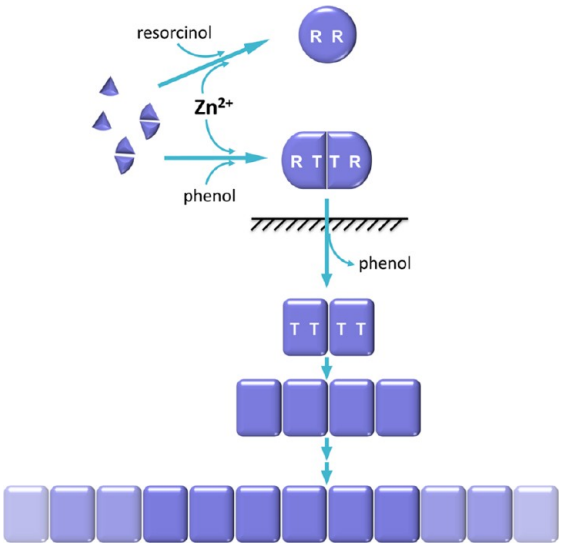

Figure 11. Cartoon model of the ligand-dependent self-association of IDeg. Formation of hexamers in the presence of zinc and resorcinol, dihexamers in the presence of zinc and phenol, and linear multihexamers upon depletion of phenol. The quaternary states are tightly linked to the conformational state of the protomer. The barrier indicated by black slashes represents the transition from solvent conditions in the pharmaceutical formulation to the solvent conditions in the sub cutis after injection.

conformation. The phenolic ligand acts as a molecular switch such that upon injection of the formulation and subsequent dissociation of the phenolic ligand a concomitant conformational change takes place. This, in turn, prompts the formation of supramolecular structures of multihexamers that form a soluble depot of IDeg. The multihexamers are composed of linear arrays of hundreds of hexamers in the T_6 conformation. The transition between dihexamers and multihexamers is governed by the classical principles of Monod for quaternary assemblies of asymmetric and symmetric protomers,[60] corresponding to the T_3R_3 protomers and T_6 protomers of the dihexamer and the multihexamer, respectively. Moreover, the unprecedented $R_3T_3-T_3R_3$ structure and the linear self-assembly of IDeg with tight linkage of conformational states and formation of quaternary structure originate in the allosteric properties of insulin and its tendency for half-site reactivity.[26] The zinc assemblies of IDeg provide the basis for the novel concept for protraction of insulin and have allowed the development of insulin degludec possessing an ultralong glucose-lowering effect.[13]

■ ASSOCIATED CONTENT

Supporting Information

SV−AUC and SE−AUC data of zinc-free IDeg, SE−AUC data of IDeg in the presences of zinc and phenol, 1D ^{1}H NMR spectroscopy data of zinc-free IDeg, NUV-CD data of the conformational change of HI in the presence of zinc and resorcinol, simulation of circular dichroism data based on species distribution, FTIR spectroscopy data of films of zinc complexes of IDeg with and without phenol, SV−AUC and SE−AUC data of zinc complexes of IDeg without phenol, and NUV-CD data of the conformation of zinc complexes of IDeg without phenol. This material is available free of charge via the Internet at http://pubs.acs.org.

■ AUTHOR INFORMATION

Corresponding Author

*Phone: +45 30752583. E-mail: dbs@novonordisk.com.

Notes

The authors are all employed by and own stock in Novo Nordisk A/S.

■ ACKNOWLEDGMENTS

We thank Ane Margrethe Blom, Berit Bergerud Hansen, Berit Bugge Nielsen, Henning Gustafsson, Lene Drube, Tina Østergaard, and Ulrich Ehrbar for expert technical assistance and without whom this work would not have been possible. We thank the staff of synchrotron beamlines X33 at EMBL (Hamburg, Germany), X06SA at the Swiss Light source (Villigen, Switzerland), and I911-3 at MaxLab (Lund, Sweden) for assistance with collecting the diffraction and SAXS data. We are also grateful to Helle Birk Olsen and Svend Ludvigsen for valuable discussion.

■ ABBREVIATIONS

AUC, analytical ultracentrifugation; CD, circular dichroism; HI, human insulin; IDeg, insulin degludec or Lys^{B29}(N^{ε}-hexadecandioyl)-γ-L-glutamic acid des(B30) human insulin; SAXS, small-angle X-ray scattering; SE, sedimentation equilibrium; SV, sedimentation velocity; TEM, transmission electron microscopy; wwPDB, worldwide Protein Data Bank; Zn^{2+}/6Ins, molar ratio of zinc acetate to insulin, either human insulin or insulin degludec as indicated.

■ REFERENCES

(1) DeFelippis, M. R., Chance, R. E., and Frank, B. H. (2001) Insulin self-association and the relationship to pharmacokinetics and pharmacodynamics. *Crit. Rev. Ther. Drug Carrier Syst. 18*, 201−264.

(2) Brange, J., Ribel, U., Hansen, J. F., Dodson, G., Hansen, M. T., Havelund, S., Melberg, S. G., Norris, F., Norris, K., Snel, L., Soerensen, A. R., and Voight, H. O. (1988) Monomeric insulins obtained by protein engineering and their medical implications. *Nature 333*, 679−682.

(3) Brange, J., and Volund, A. (1999) Insulin analogs with improved pharmacokinetic profiles. *Adv. Drug Delivery Rev. 35*, 307−335.

(4) Brems, D. N., Alter, L. A., Beckage, M. J., Chance, R. E., DiMarchi, R. D., Green, L. K., Long, H. B., Pekar, A. H., Shields, J. E., and Frank, B. H. (1992) Altering the association properties of insulin by amino acid replacement. *Protein Eng. 5*, 527−533.

(5) Kurtzhals, P., Havelund, S., Jonassen, I., Kiehr, B., Larsen, U. D., Ribel, U., and Markussen, J. (1995) Albumin binding of insulins acylated with fatty acids: Characterization of the ligand-protein interaction and correlation between binding affinity and timing of the insulin effect in vivo. *Biochem. J. 312*, 725−731.

(6) Jonassen, I., Havelund, S., Ribel, U., Plum, A., Loftager, M., Hoeg-Jensen, T., Volund, A., and Markussen, J. (2006) Biochemical and physiological properties of a novel series of long-acting insulin analogs obtained by acylation with cholic acid derivatives. *Pharm. Res. 23*, 49−55.

(7) Olsen, H. B., and Kaarsholm, N. C. (2000) Structural effects of protein lipidation as revealed by LysB29-myristoyl, des(B30) insulin. *Biochemistry 39*, 11893−11900.

(8) Havelund, S., Plum, A., Ribel, U., Jonassen, I., Volund, A., Markussen, J., and Kurtzhals, P. (2004) The mechanism of protraction of insulin detemir, a long-acting, acylated analog of human insulin. *Pharm. Res. 21*, 1498−1504.

(9) Clodfelter, D. K., Pekar, A. H., Rebhun, D. M., Destrampe, K. A., Havel, H. A., Myers, S. R., and Brader, M. L. (1998) Effects of non-covalent self-association on the subcutaneous absorption of a therapeutic peptide. *Pharm. Res. 15*, 254−262.
(10) Steensgaard, D. B., Thomsen, J. K., Olsen, H. B., and Knudsen, L. B. (2008) The molecular basis for the delayed absorption of the once-daily human GLP-1 analogue, liraglutide. *Diabetes 57* (Suppl. 1), A164.
(11) Birkeland, K. I., Home, P. D., Wendisch, U., Ratner, R. E., Johansen, T., Endahl, L. A., Lyby, K., Jendle, J. H., Roberts, A. P., DeVries, J. H., and Meneghini, L. F. (2011) Insulin degludec in type 1 diabetes: A randomized controlled trial of a new-generation ultra-long-acting insulin compared with insulin glargine. *Diabetes Care 34*, 661−665.
(12) Heise, T., Tack, C. J., Cuddihy, R., Davidson, J., Gouet, D., Liebl, A., Romero, E., Mersebach, H., Dykiel, P., and Jorde, R. (2011) A new-generation ultra-long-acting basal insulin with a bolus boost compared with insulin glargine in insulin-naive people with type 2 diabetes: A randomized, controlled trial. *Diabetes Care 34*, 669−674.
(13) Jonassen, I., Havelund, S., Hoeg-Jensen, T., Steensgaard, D. B., Wahlund, P. O., and Ribel, U. (2012) Design of the Novel Protraction Mechanism of Insulin Degludec, an Ultra-long Acting Basal Insulin. *Pharm. Res. 29*, 2104−2114.
(14) Dunn, M. F. (2005) Zinc-ligand interactions modulate assembly and stability of the insulin hexamer: A review. *BioMetals 18*, 295−303.
(15) Ludvigsen, S., Roy, M., Thogersen, H., and Kaarsholm, N. C. (1994) High-resolution structure of an engineered biologically potent insulin monomer, B16 Tyr → His, as determined by nuclear-magnetic-resonance spectroscopy. *Biochemistry 33*, 7998−8006.
(16) Olsen, H. B., Ludvigsen, S., and Kaarsholm, N. C. (1996) Solution structure of an engineered insulin monomer at neutral pH. *Biochemestry 35*, 8836−8845.
(17) Jorgensen, A. M., Kristensen, S. M., Led, J. J., and Balschmidt, P. (1992) Three-dimensional solution structure of an insulin dimer. A study of the B9(Asp) mutant of human insulin using nuclear magnetic resonance, distance geometry and restrained molecular dynamics. *J. Mol. Biol. 227*, 1146−1163.
(18) Adams, M. J., Blundell, T. L., Dodson, E. J., Dodson, G. G., Vijayan, M., Baker, E. N., Harding, M. M., Hodgkin, D. C., Rimmer, B., and Sheat, S. (1969) Structure of Rhombohedral 2 Zinc Insulin Crystals. *Nature 224*, 491−495.
(19) Smith, G. D., Swenson, D. C., Dodson, E. J., Dodson, G. G., and Reynolds, C. D. (1984) Structural Stability in the 4-zinc Human Insulin Hexamer. *Proc. Natl. Acad. Sci. U.S.A. 81*, 7093−7097.
(20) Kaarsholm, N. C., Ko, H.-C., and Dunn, M. F. (1989) Comparison of Solution Structural Flexibility and Zinc Binding Domains for Insulin, Proinsulin, and Miniproinsulin. *Biochemistry 28*, 4427−4435.
(21) Dodson, G. G., Cutfield, S., Hoenjet, E., Wollmer, A., and Brandenburg, D. (1979) Crystal Structure, Aggregation, and Biological Potency of Beef Insulin Cross Linked at A1 and B29 by Diaminosuberic Acid. In *Insulin: Chemistry, Structure, and Function of Insulin and Related Hormones. Proceedings of the Second International Insulin Symposium* (Brandenburg, D., and Wollmer, A., Eds.) pp 17−26, Aachen, Germany, September 4−7, De Gruyter, Berlin.
(22) Huang, S. T., Choi, W. E., Bloom, C., Leuenberger, M., and Dunn, M. F. (1997) Carboxylate ions are strong allosteric ligands for the HisB10 sites of the R-state insulin hexamer. *Biochemistry 36*, 9878−9888.
(23) Rahuel-Clermont, S., French, C. A., Kaarsholm, N. C., Dunn, M. F., and Chou, C. I. (1997) Mechanisms of stabilization of the insulin hexamer through allosteric ligand interactions. *Biochemistry 36*, 5837−5845.
(24) Seydoux, F., Malhotra, O. P., Bernhard, S. A., and Stark, G. (1974) Half-Site Reactivity. *Crit. Rev. Biochem. Mol. Biol. 2*, 227−257.
(25) Bloom, C. R., Choi, W. E., Brzovic, P. S., Ha, J. J., Huang, S. T., Kaarsholm, N. C., and Dunn, M. F. (1995) Ligand binding to wild-type and E-B13Q mutant insulins: A three-state allosteric model system showing half-site reactivity. *J. Mol. Biol. 245*, 324−330.
(26) Bloom, C. R., Kaarsholm, N. C., Ha, J., and Dunn, M. F. (1997) Half-site reactivity, negative cooperativity, and positive cooperativity: Quantitative considerations of a plausible model. *Biochemistry 36*, 12759−12765.
(27) Kabsch, W. (2010) XDS. *Acta Crystallogr. D66*, 125−132.
(28) Otwinowski, Z., and Minor, W. (1997) Processing of X-ray diffraction data. *Methods Enzymol. 276*, 307−326.
(29) Bailey, S. (1994) The CCP4 suite: Programs for protein crystallography. *Acta Crystallogr. D50*, 760−763.
(30) Adams, P. D., Grosse-Kunstleve, R. W., Hung, L. W., Ioerger, T. R., McCoy, A. J., Moriarty, N. W., Read, R. J., Sacchettini, J. C., Sauter, N. K., and Terwilliger, T. C. (2002) PHENIX: Building new software for automated crystallographic structure determination. *Acta Crystallogr. D58*, 1948−1954.
(31) Schuck, P. (2000) Size-distribution analysis of macromolecules by sedimentation velocity ultracentrifugation and Lamm equation modeling. *Biophys. J. 78*, 1606−1619.
(32) Stafford, W. F., III (1992) Boundary analysis in sedimentation transport experiments: A procedure for obtaining sedimentation coefficient distributions using the time derivative of the concentration profile. *Anal. Biochem. 203*, 295−301.
(33) Yphantis, D. A. (1964) Equilibrium ultracentrifugation of dilute solutions. *Biochemistry 3*, 297−317.
(34) Roessle, M. W., Klaering, R., Ristau, U., Robrahn, B., Jahn, D., Gehrmann, T., Konarev, P., Round, A., Fiedler, S., Hermes, C., and Svergun, D. (2007) Upgrade of the small-angle X-ray scattering beamline X33 at the European Molecular Biology Laboratory, Hamburg. *J. Appl. Crystallogr. 40*, 190−194.
(35) Petoukhov, M. V., Konarev, P. V., Kikhney, A. G., and Svergun, D. I. (2007) ATSAS 2.1: Towards automated and web-supported small-angle scattering data analysis. *J. Appl. Crystallogr. 40*, 223−228.
(36) Konarev, P. V., Volkov, V. V., Sokolova, A. V., Koch, M. H. J., and Svergun, D. I. (2003) PRIMUS: A Windows PC-based system for small-angle scattering data analysis. *J. Appl. Crystallogr. 36*, 1277−1282.
(37) Svergun, D. (1992) Determination of the regularization parameter in indirect-transform methods using perceptual criteria. *J. Appl. Crystallogr. 25*, 495−503.
(38) Svergun, D., Barberato, C., and Koch, M. H. J. (1995) CRYSOL: A Program to Evaluate X-ray Solution Scattering of Biological Macromolecules from Atomic Coordinates. *J. Appl. Crystallogr. 28*, 768−773.
(39) Franke, D., and Svergun, D. I. (2009) DAMMIF, a program for rapid ab-initio shape determination in small-angle scattering. *J. Appl. Crystallogr. 42*, 342−346.
(40) DeLano, W. L. (2002) *The PyMOL Molecular Graphics System*, DeLano Scientific, San Carlos, CA.
(41) Berman, H., Henrick, K., Nakamura, H., and Markley, J. L. (2007) The worldwide Protein Data Bank (wwPDB): Ensuring a single, uniform archive of PDB data. *Nucleic Acids Res. 35*, D301−D303.
(42) Diao, J. (2003) Crystallographic titration of cubic insulin crystals: pH affects GluB13 switching and sulfate binding. *Acta Crystallogr. D59*, 670−676.
(43) Schachman, H. K. (1959) *Ultracentrifugation in Biochemistry*, Vol. 35, p 272, Academic Press, New York.
(44) Svedberg, T., and Pedersen, K. O. (1940) Die Ultrazentrifuge. In *Handbuch der Kolloidwissenschaft*, Vol. 8, Steinkopff, Dresden.
(45) Chervenka, C. H. (1969) *A Manual of Methods for the Analytical Ultracentrifuge*, Spinco Division of Beckman Instruments, Palo Alto, CA.
(46) Attri, A. K., Fernandez, C., and Minton, A. P. (2010) pH-dependent self-association of zinc-free insulin characterized by concentration-gradient static light scattering. *Biophys. Chem. 148*, 28−33.
(47) Jeffrey, P. D., Milthorpe, B. K., and Nichol, L. W. (1976) Polymerization pattern of insulin at pH 7.0. *Biochemistry 15*, 4660−4665.

(48) Mark, A. E., and Jeffrey, P. D. (1990) The self-association of zinc-free bovine insulin. Four model patterns and their significance. *Biol. Chem. Hoppe-Seyler 371*, 1165−1174.
(49) Smith, G. D., Ciszak, E., Magrum, L. A., Pangborn, W. A., and Blessing, R. H. (2000) R6 hexameric insulin complexed with m-cresol or resorcinol. *Acta Crystallogr. D56*, 1541−1548.
(50) Bentley, G., Dodson, G., and Lewitova, A. (1978) Rhombohedral insulin crystal transformation. *J. Mol. Biol. 126*, 871−875.
(51) Wagner, A., Diez, J., Schulze-Briese, C., and Schluckebier, G. (2009) Crystal structure of ultralente: A microcrystalline insulin suspension. *Proteins 74*, 1018−1027.
(52) Whittingham, J. L., Chaudhuri, S., Dodson, E. J., Moody, P. C., and Dodson, G. G. (1995) X-ray crystallographic studies on hexameric insulins in the presence of helix-stabilizing agents, thiocyanate, methylparaben, and phenol. *Biochemistry 34*, 15553−15563.
(53) Chayen, N. E., Stewart, P. D. S., and Blow, D. M. (1992) Microbatch crystallization under oil. A new technique allowing many small-volume crystallization trials. *J. Cryst. Growth 122*, 176−180.
(54) Brader, M. L., Kaarsholm, N. C., Lee, R. W., and Dunn, M. F. (1991) Characterization of the R-state insulin hexamer and its derivatives. The hexamer is stabilized by heterotropic ligand binding interactions. *Biochemistry 30*, 6636−6645.
(55) Kruger, P., Gilge, G., Cabuk, Y., and Wollmer, A. (1990) Cooperativity and intermediate states in the T-R-structural transformation of insulin. *Biol. Chem. Hoppe-Seyler 371*, 669−673.
(56) Jimenez, J. L., Nettleton, E. J., Bouchard, M., Robinson, C. V., Dobson, C. M., and Saibil, H. R. (2002) The protofilament structure of insulin amyloid fibrils. *Proc. Natl. Acad. Sci. U.S.A. 99*, 9196−9201.
(57) Harding, S. E. (1992) Sedimentation analysis of polysaccharides. In *Analytical Ultracentrifugation in Biochemistry and Polymer Science*, pp 495−516, The Royal Society of Chemistry, Nottingham, U.K.
(58) Uversky, V. N. (2002) What does it mean to be natively unfolded? *Eur. J. Biochem. 269*, 2−12.
(59) Whittingham, J. L., Havelund, S., and Jonassen, I. (1997) Crystal structure of a prolonged-acting insulin with albumin-binding properties. *Biochemistry 36*, 2826−2831.
(60) Monod, J., Wyman, J., and Changeux, J.-P. (1965) On the nature of allosteric transitions: A plausible model. *J. Mol. Biol. 12*, 88−118.
(61) Hvidt, S. (1991) Insulin association in neutral solutions studied by light scattering. *Biophys. Chem. 39*, 205−213.
(62) Attri, A. K., Fernandez, C., and Minton, A. P. (2010) Self-association of Zn-insulin at neutral pH: Investigation by concentration gradient-static and dynamic light scattering. *Biophys. Chem. 148*, 23−27.
(63) Phillips, N. B., Wan, Z. L., Whittaker, L., Hu, S. Q., Huang, K., Hua, Q. X., Whittaker, J., Ismail-Beigi, F., and Weiss, M. A. (2010) Supramolecular protein engineering: Design of zinc-stapled insulin hexamers as a long acting depot. *J. Biol. Chem. 285*, 11755−11759.